nature nanotechnology

ARTICLES

https://doi.org/10.1038/s41565-018-0342-5

Endosomolytic polymersomes increase the activity of cyclic dinucleotide STING agonists to enhance cancer immunotherapy

Daniel Shae[1], Kyle W. Becker[1], Plamen Christov[2], Dong Soo Yun[3], Abigail K. R. Lytton-Jean[3], Sema Sevimli[1], Manuel Ascano[4,5], Mark Kelley[6,7], Douglas B. Johnson[7,8], Justin M. Balko[7,8,9] and John T. Wilson[1,2,7,10,11,12,13]*

Cyclic dinucleotide (CDN) agonists of stimulator of interferon genes (STING) are a promising class of immunotherapeutics that activate innate immunity to increase tumour immunogenicity. However, the efficacy of CDNs is limited by drug delivery barriers, including poor cellular targeting, rapid clearance and inefficient transport to the cytosol where STING is localized. Here, we describe STING-activating nanoparticles (STING-NPs)—rationally designed polymersomes for enhanced cytosolic delivery of the endogenous CDN ligand for STING, 2′3′ cyclic guanosine monophosphate–adenosine monophosphate (cGAMP). STING-NPs increase the biological potency of cGAMP, enhance STING signalling in the tumour microenvironment and sentinel lymph node, and convert immunosuppressive tumours to immunogenic, tumoricidal microenvironments. This leads to enhanced therapeutic efficacy of cGAMP, inhibition of tumour growth, increased rates of long-term survival, improved response to immune checkpoint blockade and induction of immunological memory that protects against tumour rechallenge. We validate STING-NPs in freshly isolated human melanoma tissue, highlighting their potential to improve clinical outcomes of immunotherapy.

Immune checkpoint blockade (ICB) is revolutionizing the treatment of a diversity of cancers and can yield complete and durable responses[1,2]. These remarkable outcomes provide evidence that the immune system can be harnessed to combat metastatic disease. However, patients often do not respond to Food and Drug Administration-approved ICB antibodies[1–3], invigorating a fervour of investigation into strategies to increase the number of patients that will benefit from immunotherapy[4,5]. For many tumour types, patient survival and responses to ICB correlate with an immunogenic ('hot') tumour microenvironment (TME) infiltrated with tumour antigen-specific T cells (primarily $CD8^+$ T cells) that are reactivated in response to checkpoint blockade antibodies[6–8]. However, many patients have immunologically 'cold' tumours that lack significant T-cell infiltration and are instead characterized by high densities of immunosuppressive cells that inhibit antitumour immunity. This has motivated the need for strategies to reprogramme 'cold' tumours towards immunogenic, pro-inflammatory states that reinvigorate antitumour T-cell responses.

Stimulator of interferon genes (STING) is a cytosolic pattern recognition receptor that is critical for spontaneous induction of antitumour T-cell immunity[9,10]. The STING pathway is activated in response to tumour-derived DNA in the cytoplasm, which is detected by the enzyme cyclic-GMP-AMP synthase[11–14], leading to the production of 2′,5-3′5′ cyclic guanosine monophosphate–adenosine monophosphate (cGAMP), the endogenous and high-affinity ligand for STING[15,16]. Activation of STING triggers a multifaceted type I interferon (IFN-I)-driven inflammatory programme that stimulates dendritic cell activation and cross-presentation of tumour antigen for the subsequent priming of antitumour T cells[17]. Accordingly, STING-deficient mice have a higher susceptibility to tumour formation, diminished antitumour T-cell immunity and impaired responses to immunotherapy[9,18,19]. The critical role of STING in cancer immune surveillance has motivated recent investigations leveraging cGAMP and structurally related cyclic dinucleotide (CDN) STING agonists as therapeutics to stimulate antitumour immunity[20–24]. While promising, the activity and therapeutic efficacy of exogenously delivered cGAMP—an anionic, highly water-soluble molecule—are limited by its low bioavailability and poor drug-like properties. As a result, cGAMP does not readily cross the cellular plasma membrane, is poorly endocytosed and, critically, has limited access to the cytosol where STING is located[25,26]. Moreover, CDNs are rapidly cleared with modest delivery to tumours and/or lymphoid organs[27,28].

The activity of CDNs is further limited by a lack of drug carriers optimized for this unique class of compound[29]. Here, we address the challenges limiting the therapeutic impact of CDNs through the design of a STING-activating nanoparticle (STING-NP) based on polymer vesicles (polymersomes) engineered for efficient cytosolic delivery of cGAMP (Fig. 1a,b). Through control of polymer properties, formulation methodologies and an in situ vesicle membrane

[1]Department of Chemical and Biomolecular Engineering, Vanderbilt University, Nashville, TN, USA. [2]Vanderbilt Institute of Chemical Biology, Vanderbilt University, Nashville, TN, USA. [3]The David H. Koch Institute for Integrative Cancer Research, Massachusetts Institute of Technology, Cambridge, MA, USA. [4]Department of Pathology, Microbiology and Immunology, Vanderbilt University Medical Center, Nashville, TN, USA. [5]Department of Biochemistry, Vanderbilt University Medical Center, Nashville, TN, USA. [6]Department of Surgery, Vanderbilt University Medical Center, Nashville, TN, USA. [7]Vanderbilt-Ingram Cancer Center, Nashville, TN, USA. [8]Department of Medicine, Vanderbilt University Medical Center, Nashville, TN, USA. [9]Breast Cancer Research Program, Vanderbilt University Medical Center, Nashville, TN, USA. [10]Department of Biomedical Engineering, Vanderbilt University, Nashville, TN, USA. [11]Vanderbilt Center for Immunobiology, Vanderbilt University Medical Center, Nashville, TN, USA. [12]Vanderbilt Institute for Infection, Immunology and Inflammation, Vanderbilt University Medical Center, Nashville, TN, USA. [13]Vanderbilt Institute of Nanoscale Science and Engineering, Vanderbilt University, Nashville, TN, USA. *e-mail: john.t.wilson@vanderbilt.edu

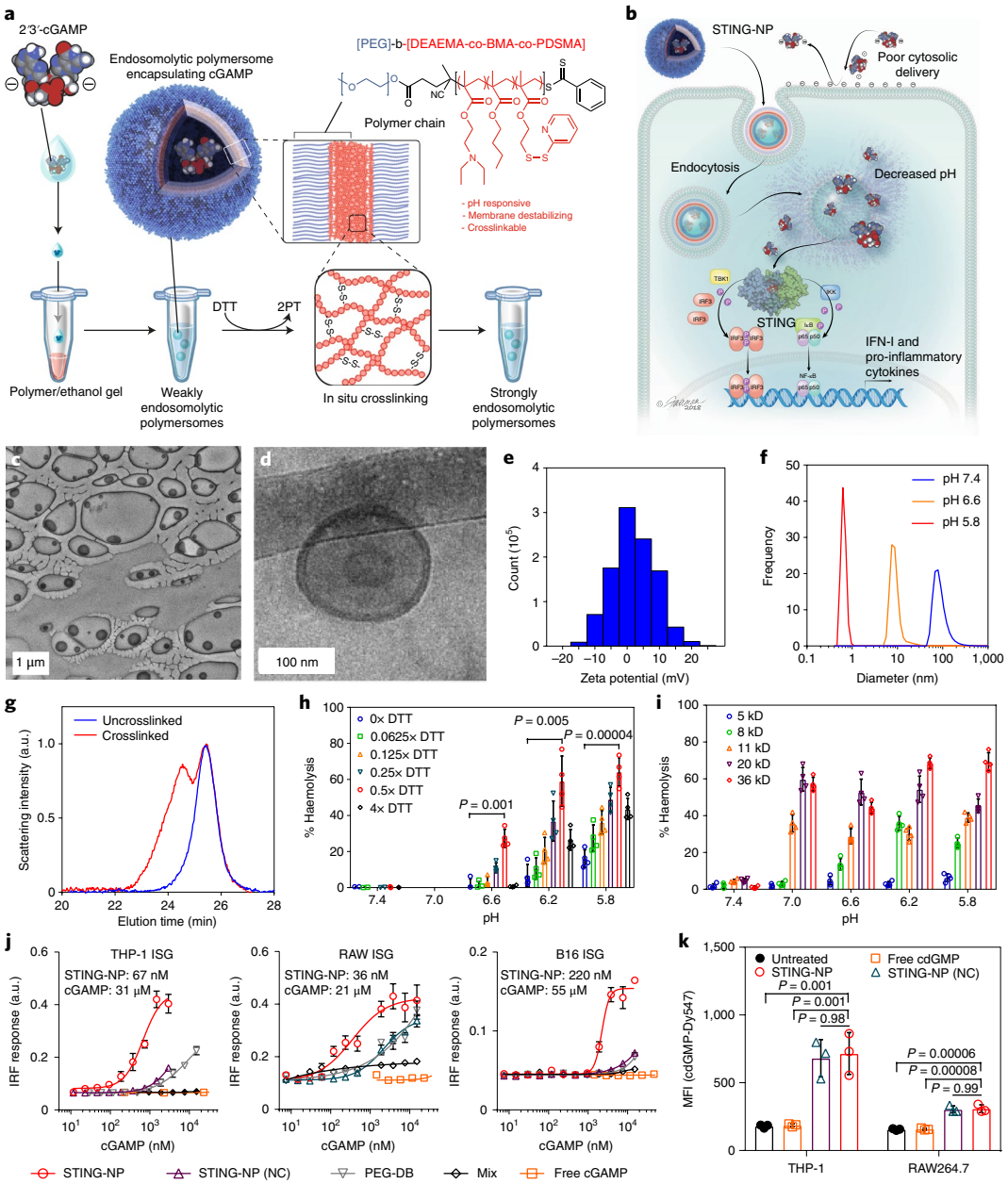

Fig. 1 | Design, optimization and characterization of STING-NPs. a, Schematic of the STING-NP structure and strategy for enhancing intracellular delivery of 2′3′-cGAMP. cGAMP is encapsulated in endosomolytic polymersomes assembled from pH-responsive diblock copolymers. After polymersome self-assembly and cGAMP loading, polymer chains are crosslinked in situ via partial reduction of pyridyl disulfide groups with DTT, resulting in the formation of disulfide crosslinks. 2PT, 2-pyridinethione. **b**, STING-NPs enhance intracellular uptake of cGAMP and, in response to decreased pH within endosomal compartments, disassemble and promote endosomal escape of cGAMP to the cytosol. IKK, IκB kinase; IκB, inhibitor of κB; IRF3, IFN regulatory factor 3; TBK1, TANK-binding kinase 1. **c**,**d**, Representative conventional (**c**) and cryogenic (**d**) transmission electron micrographs of polymersomes assembled using PEG_{2kDa}-$DBP_{4.5kDa}$ polymers. Cryogenic electron microscopy was performed once, while conventional electron microscopy was conducted independently three times with similar results. **e**, Zeta potential distribution of polymersomes at pH 7.4. The experiment was conducted independently three times with similar results. **f**, Dynamic light scattering analysis of the average particle size distribution of STING-NPs at extracellular (7.4) and endosomal (<6.6) pH. The experiment was conducted independently three times with similar results. **g**, Gel permeation chromatograms of PEG_{2kDa}-$DBP_{4.5kDa}$ copolymers before and after in situ crosslinking of polymersomes. The experiment was conducted three times independently with similar results. **h**, Effect of the degree of crosslinking, represented by equivalents of DTT to PDSMA, on pH-dependent membrane-destabilizing activity, as measured by erythrocyte haemolysis assay ($n = 4$ biologically independent samples; two-tailed Student's t-test). **i**, Effect of second block molecular weight (MW) in PEG_{2kDa}-DB_{MW} copolymers on pH-dependent haemolysis ($n = 4$ biologically independent samples). **j**, Dose–response curves of the IFN-I response elicited by indicated cGAMP-containing formulations in THP-1, RAW 264.7 and B16 ISG cells with an IFN regulatory factor (IRF)-inducible reporter construct. The EC_{50} of STING-NP and cGAMP is indicated for each cell type. Mix, physical mixture of empty crosslinked PEG_{2kDa}-b-$DBP_{4.5kDa}$ polymersomes and free cGAMP; NC, non-crosslinked; PEG-DB, cGAMP delivered with polymersomes assembled using non-crosslinkable PEG_{2kDa}-DB_{5kDa} chains ($n = 4$ biologically independent samples). **k**, Flow cytometric quantification of the uptake of cdGMP-Dy547 co-delivered with cGAMP in the indicated formulation by THP-1 and RAW 264.7 cells ($n = 3$ biologically independent samples; one-way analysis of variance (ANOVA) with Tukey test). MFI, median fluorescence intensity. All statistical data are presented as means ± s.d. Credit: ©Fairman Studios, LLC, 2018 (**a**,**b**).

crosslinking strategy, cGAMP is efficiently encapsulated into polymersomes that disassemble in response to endolysosomal acidification to unveil membrane-destabilizing polymer segments that promote endosomal escape of cGAMP. Consequently, STING-NPs enhance the biological activity of cGAMP by two to three orders of magnitude in multiple immunologically relevant cell types and trigger an IFN-I-driven innate immune response that induces a shift to a 'hot' T cell-inflamed TME. STING-NPs increase the therapeutic efficacy of cGAMP and improve responses to ICB in a poorly immunogenic murine melanoma model when administered via either an intratumoral or intravenous route. Moreover, we validate the activity of STING-NPs in resected human metastatic melanoma tissue, demonstrating the translational potential of STING-NPs as a platform for increasing tumour immunogenicity.

Results and discussion

Design of endosomolytic polymersomes for cytosolic delivery of cGAMP. To optimize STING-NPs for cGAMP delivery, we designed polymersomes with an aqueous core for efficient hydrophilic drug loading and a vesicle membrane comprising amphiphilic diblock copolymer chains with pH-responsive, membrane-destabilizing activity to mediate the intracellular release and endosomal escape of cGAMP (Fig. 1a,b). We synthesized well-defined poly(ethylene glycol)-block-[(2-(diethylamino)ethyl methacrylate)-co-(butyl methacrylate)-co-(pyridyl disulfide ethyl methacrylate)] (PEG-DBP) copolymers using reversible addition-fragmentation chain transfer polymerization. pH-sensitive, cationic 2-(diethylamino) ethyl methacrylate (DEAEMA) groups and hydrophobic butyl methacrylate (BMA) moieties were integrated at a molar ratio previously reported to be optimal for endosomal escape[30,31]. Thiol-reactive pyridyl disulfide ethyl methacrylate (PDSMA) groups were copolymerized into the second block for in situ crosslinking of chains within the vesicle membrane via partial reduction with dithiothreitol (DTT). To achieve high encapsulation efficiencies, polymersomes were formulated via a modified direct hydration method[32] that enables a high volume ratio of polymer to encapsulant during the vesicle assembly process.

The resulting particles were PEGylated, surface-neutral vesicles with a median hydrodynamic diameter of ~80 nm at pH 7.4 (Fig. 1c–e). The polymerization conditions were chosen to incorporate an average of around two PDSMA groups per chain, to prevent the formation of a fully crosslinked network structure within polymersomes. Polymersomes therefore retained pH-responsive disassembly after crosslinking, as demonstrated by a decrease in nanoparticle diameter at endosomal pH (Fig. 1f). Chain crosslinking was observed directly via an increase in molecular weight (number average molar mass, $M_n = 11$ kDa; polydispersity index = 1.2) (Fig. 1g) and the release of 2-pyridinethione (Supplementary Fig. 1a). No evidence of interparticle crosslinking was observed in dynamic light scattering analysis of particles before and after crosslinking (Supplementary Fig. 1b–d).

Next, we evaluated the pH-responsive, membrane-destabilizing activity of polymersomes using an erythrocyte haemolysis assay that is commonly used to predict the endosomolytic activity of drug carriers[33,34]. Vesicle membrane crosslinking enhanced the haemolytic activity at endosomal pH relative to uncrosslinked variants (Fig. 1h), probably due to an increased average molecular weight of the membrane-destabilizing DBP polymer blocks on crosslinking (Fig. 1g). This is consistent with findings that the pH-dependent haemolytic activity of PEG-b-[DEAEMA-co-BMA] (PEG-DB) polymers correlates positively with increasing molecular weight of the DB block (Fig. 1i). While weakly haemolytic PEG_{2kDa}-DB_{5kDa} and PEG_{2kDa}-$DBP_{4.5kDa}$ polymers self-assembled into polymersomes that encapsulated cGAMP, all larger PEG_{2kDa}-$DB_{8–36kDa}$ polymers formed poorly defined, colloidally unstable aggregates (Supplementary Table 1), consistent with a weight fraction of PEG less than 0.25 for which vesicle assembly is not expected[35]. To determine whether haemolytic activity could be increased while maintaining a vesicular structure, we synthesized PEG-DB with larger (5 and 10 kDa) PEG blocks. However, these polymers assembled into worm-like or spherical micelles (Supplementary Fig. 2), probably driven by increased steric repulsion in polymer chains with long PEG coronas—a well-documented effect that disfavours vesicular self-assembly due to the relatively low surface curvature of bilayer structures[36,37]. Without aqueous cores, micellar morphologies demonstrated lower cGAMP loading than PEG_{2kDa}-DBP_{5kDa} vesicles. These results reveal an inherent tension between achieving potent endosomolytic activity and the assembly of cGAMP-loaded PEG-DB vesicles, and motivated the use of low-molecular-weight PEG_{2kDa}-$DBP_{4.5kDa}$ polymer chains in conjunction with in situ vesicle crosslinking in the design of STING-NPs.

STING-NPs increase the immunostimulatory potency of 2′3′-cGAMP. Given the critical role of IFN-I in antitumour immunity[38], we evaluated the ability of STING-NPs to stimulate IFN-I responses in monocyte, macrophage and melanoma cell lines (Fig. 1j). The delivery of cGAMP in crosslinked PEG-DBP vesicles increased cGAMP activity by several orders of magnitude (half-maximum effective concentration (EC_{50}) = 67 ± 12, 36 ± 14 and 230 ± 1.0 nM in THP-1 (monocyte), RAW 264.7 (macrophage) and B16 (melanoma) IFN-stimulated gene (ISG) cell lines, respectively), whereas free cGAMP elicited little response, even at high concentrations (EC_{50} = 31 ± 1, 22 ± 4 and 55 ± 2 μM, respectively). A similar enhancement in cGAMP potency was observed in both DC2.4 dendritic cells and bone marrow-derived dendritic cells (Supplementary Fig. 3). We observed a relationship between haemolytic activity at endosomal pH values and increased STING-NP activity, as weakly haemolytic PEG-DB and uncrosslinked PEG-DBP vesicles only modestly increased cGAMP activity.

Mixing cGAMP with pre-formulated vesicles resulted in a negligible increase in activity, indicating that cGAMP encapsulation was critical to efficient STING activation. This finding was further supported by evaluating the activity of PEG-DB polymers that did not form vesicular structures. Although we observed some association between cGAMP and the micellar structures formed using higher-molecular-weight PEG-DB polymers, we found that these morphologies mediated minimal enhancements in cGAMP activity despite being highly haemolytic (Supplementary Fig. 4). This highlights an important distinction between the delivery of oligonucleotide therapeutics (for example, small interfering RNA), which can be stably complexed to cationic carriers via a multivalent electrostatic interaction[39], and CDNs, which may lack a sufficient degree of charge for stable electrostatic complexation with DEAEMA groups.

We next evaluated the capacity of polymersomes to enhance the cellular uptake of cGAMP by co-encapsulating cGAMP with a fluorescently labelled CDN (cdGMP-Dy547). While cdGMP-Dy547 uptake varied between cell types, STING-NPs increased uptake by ~1.5–3.5×, with no significant differences observed between crosslinked and uncrosslinked STING-NPs (Fig. 1k). While some increase in cGAMP activity can be attributed to enhanced intracellular uptake, the magnitude of reduction in EC_{50} achieved with STING-NPs is probably primarily a consequence of enhanced endosomal escape and cytosolic delivery of cGAMP. Hence, by combining precisely designed diblock copolymers, a formulation method that enables high cGAMP encapsulation efficiency (~38%) and vesicle membrane crosslinking to enhance endosomolytic activity, STING-NPs enhance the cGAMP potency 240–610-fold—one of the largest carrier-mediated fold increases in CDN activity reported to date[26,40].

Next, subcutaneous B16.F10 melanoma tumours (~100 mm^3) grown in immunocompetent mice were treated via intratumoral injection with STING-NP, free cGAMP or vehicle (phosphate

buffered saline (PBS)) and harvested 4 h later for quantitative PCR (qPCR) gene expression analysis. Compared with free cGAMP and vehicle, STING-NPs increased the expression of *Ifnb1* (6.3-fold over free cGAMP), *Cxcl9* (6.6-fold) and *Cxcl10* (4.9-fold) (Fig. 2a), which are critical mediators of antitumour T-cell activation and recruitment[17,41]. Similar to previous reports[21], *Ifnb1* expression was highly variable at 4 h, probably due to tumour heterogeneity and tight temporal regulation of gene expression levels. Nonetheless, there was a positive linear correlation between *Ifnb1* and *Cxcl9* levels, and between *Ifnb1* and *Cxcl10* levels, in treated mice (Supplementary Fig. 5), consistent with a STING-driven inflammatory response. IFN-mediated inflammation was further monitored through longitudinal optical imaging using tumours expressing an IFN-stimulated response element (ISRE) luciferase reporter. A single STING-NP treatment resulted in an elevated and extended IFN response in the tumour, while free cGAMP did not elicit a response above the baseline (Fig. 2b). Intratumoral administration of STING-NPs was well tolerated, with mice exhibiting minimal, transient weight loss. Analysis of blood chemistry and liver histology revealed no evidence of liver or kidney toxicity caused by STING-NPs (Supplementary Fig. 6).

We further characterized the gene expression profiles using multiplexed gene expression analysis (NanoString; Fig. 2c–e and Supplementary Fig. 7). Of >700 genes, the expression levels of *Il6* and *Ifnb1* were most significantly upregulated (~1,000-fold) relative to vehicle controls, consistent with STING-mediated IFN regulatory factor 3 and NF-κB (nuclear factor kappa-light-chain-enhancer of activated B cells) signalling[16]. More generally, STING-NPs triggered a multifaceted shift to an inflamed and tumoricidal microenvironment, with significant upregulation of ISGs, pro-inflammatory cytokines, leukocyte-recruiting chemokines, pro-apoptotic mediators, genes associated with dendritic cell maturation and T-cell priming, and markers of natural killer cell and T-cell activation (Fig. 2c). Several immunosuppressive mediators were also upregulated, which probably act as endogenous negative regulators of STING activation[16]. Some of these genes are the targets of pharmaceuticals that are either clinically advanced (for example, programmed death-ligand 1 (PD-L1) and indoleamine 2,3-dioxygenase 1 (IDO-1)) or in development (for example, interleukin 10 (IL-10) and arginase 2) and are potential candidates for combination therapy with STING-NPs. While not explored herein, an attractive feature of STING-NPs is the ability to efficiently encapsulate a diversity of cargo, offering opportunities for the co-delivery of CDNs with other intracellular-acting immunomodulators.

To elucidate differences between STING-NP and cGAMP treatment, the most differentially expressed genes were ranked by the fold-change expression level between STING-NP- and cGAMP-treated tumours (Fig. 2d). In selected genes, we observed a consistent 5–10-fold increase in gene expression in mice treated with STING-NP versus cGAMP, with the exception of *Cxcl1* (35-fold) and *Ifna2* (20-fold). Treatment with STING-NPs and free cGAMP elicited directionally similar changes in transcriptional profiles, suggesting a similar mechanism of action and minimal off-target effects associated with STING-NPs. This was further corroborated by unsupervised hierarchal clustering of genes with significantly different expression levels relative to the vehicle control, which revealed similar gene clusters between cGAMP- and STING-NP-treated tumours (Fig. 2e).

B16.F10 melanoma tumours were injected with STING-NPs co-loaded with cGAMP and cdGMP-Dy547 or a mixture of soluble cGAMP and cdGMP-Dy547, and flow cytometry was used to quantify the cellular uptake of cdGMP-Dy547 (Fig. 2f,g). cdGMP-Dy547 was most commonly localized in dendritic cells ($CD11c^+MHC\text{-}II^+$), natural killer cells ($CD45^+NK1.1^+$) and macrophages ($CD11b^+F4/80^+$), with STING-NPs increasing the degree of CDN uptake in natural killer cells, dendritic cells and $CD45^-$ cells. Less significant increases in STING-NP-mediated uptake were observed in macrophages ($CD11b^+F4/80^+$) and myeloid-derived suppressor cells (MDSCs) ($CD11b^+Gr\text{-}1^+$), and there was negligible uptake of both free and encapsulated CDN by T cells ($CD3^+$). Among these cells, cdGMP-Dy547 uptake was highest in natural killer cells, dendritic cells and macrophages (Fig. 2g). Cultured dendritic cells (DC2.4), macrophages (RAW 264.7), natural killer cells and B16.F10 melanoma cells were incubated with STING-NPs, and *Ifnb1* levels were measured. Macrophages and dendritic cells expressed the highest levels of *Ifnb1* in response to STING-NPs, whereas minimal expression was observed in B16.F10 tumour cells or natural killer cells (Fig. 2h). Collectively, these data indicate that macrophages and dendritic cells are the primary immunocellular targets of STING-NPs.

Lymph nodes act as command centres for orchestrating antitumour immunity, yet, like the tumour site, are often highly immunosuppressed, resulting in impaired priming of antitumour T cells[42]. Nanoparticles in the 20–100 nm range preferentially drain through the lymphatics after interstitial injection, resulting in enrichment of cargo within local draining lymph nodes[27,43,44]. Consistent with this phenomenon, STING-NPs increased cdGMP-Dy547 accumulation in the sentinel (inguinal) lymph node relative to free CDN, which was undetectable above the background (Fig. 2i). This was further supported by significant elevation of *Ifnb1* expression in the inguinal lymph node post-administration of STING-NP relative to free cGAMP, which failed to stimulate IFN-I (Fig. 2j). Therefore, in addition to their capacity for potent STING activation, another important advantage of STING-NPs—and a potential key distinction from small-molecule STING agonists—is their ability to enhance CDN uptake and STING signalling in the sentinel lymph node.

STING-NPs stimulate an immunogenic, T-cell-inflamed TME. Next, we evaluated the effect of STING-NPs on the immunocellular composition of the B16.F10 melanoma TME. A single intratumoral treatment with STING-NPs dramatically increased the number of tumour-infiltrating $CD11b^+Ly6c^+Ly6g^+$ activated neutrophils[45] relative to free cGAMP (Fig. 3a). This is consistent with the substantial increase in STING-NP-treated tumours of the neutrophil chemokine *Cxcl1* (ref. [46]). Additionally, surface expression of CD206—a canonical marker of M2-polarized macrophages—was decreased on macrophages in STING-NP-treated tumours (Fig. 3b), suggesting repolarization or recruitment of macrophages with reduced immunosuppressive capacity. Dendritic cell expression of CD86 in the tumour-draining lymph node (TDLN) (Fig. 3c) was increased, consistent with enhanced CDN accumulation in lymph nodes. Free cGAMP and STING-NPs promoted the influx of similar numbers of monocytic MDSCs with immunosuppressive potential (Fig. 3a)—probably a regulatory response to restrict STING-mediated inflammation and a potential target for combination therapy[47]. STING-NPs also significantly increased the number of infiltrating $CD8^+$ and $CD4^+$ T cells (Fig. 3d,e). Additionally, STING-NP treatment increased the $CD8^+/CD4^+$ T-cell ratio—a commonly reported prognostic indicator of the response to immunotherapy and clinical outcome (Fig. 3f)[48–50]. Ex vivo phorbol 12-myristate 13-acetate/ionomycin re-stimulation of T cells revealed that STING-NPs also significantly increased the percentage of IFN-γ- and tumour necrosis factor-α (TNF-α)-secreting $CD4^+$ T cells and TNF-α^+CD8^+ T cells in the TME relative to cGAMP, indicating enhanced antitumour functionality of infiltrating T cells in STING-NP-treated tumours (Fig. 3g). No significant changes in the percentage of $CD4^+$ or $CD8^+$ T cells secreting the immunosuppressive cytokines IL-4 and IL-10 were observed (Supplementary Fig. 8).

STING-NPs enhance the therapeutic efficacy of cGAMP. First, we evaluated therapeutic efficacy using an intratumoral administration

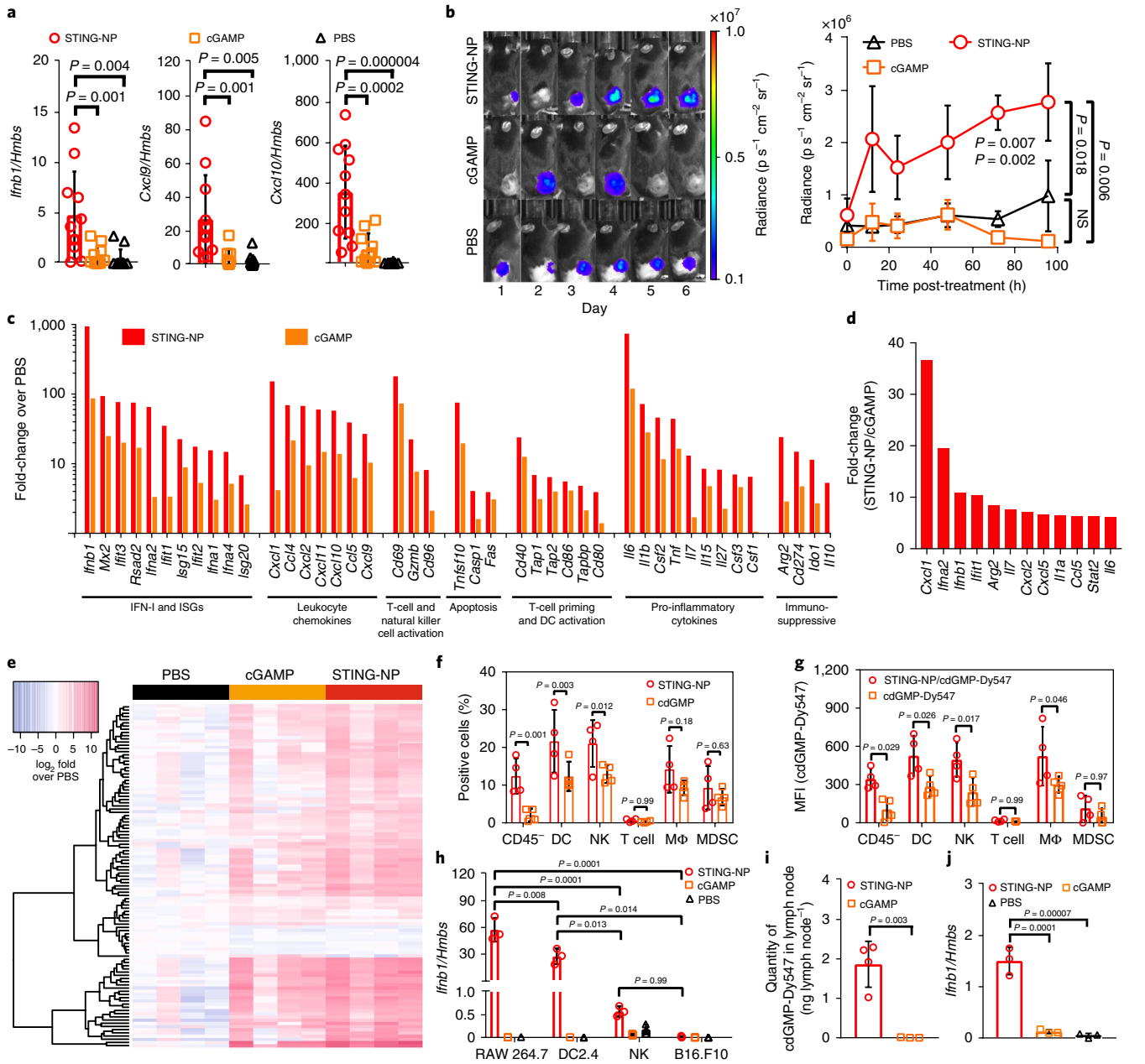

Fig. 2 | STING-NPs enhance the delivery and immunostimulatory activity of cGAMP in the TME. a, qPCR analysis of *Ifnb1*, *Cxcl9* and *Cxcl10* expression in B16.F10 tumours 4 h after intratumoral administration of STING-NP, free cGAMP or PBS as a vehicle control ($n = 11$, 10 and 12 biologically independent samples, respectively; one-way ANOVA with Tukey test) at a dose corresponding to 10 μg cGAMP. **b**, Luminescence of subcutaneous B16.F10 tumours expressing an ISRE luciferase reporter following intratumoral treatment with the indicated formulations (means ± s.e.m.; for STING-NP, cGAMP and PBS, $n = 5$, 4 and 5 biologically independent samples, respectively; two-way ANOVA with Tukey test). $P = 0.007$ and $P = 0.002$ denote the significance levels of PBS- and cGAMP-treated mice, respectively, versus STING-NP at $t = 72$ h. $P = 0.018$ and $P = 0.006$ are for PBS and cGAMP, respectively, versus STING-NP at 96 h. NS, not significant. **c**, Summary of selected differentially expressed genes ($P < 0.05$, one-way ANOVA) in response to treatment with STING-NPs or cGAMP ($n = 4$ biologically independent samples). **d**, Ranked analysis of differential gene expression between STING-NP and cGAMP administration ($n = 4$ biologically independent samples). **e**, Unsupervised hierarchical clustering of relative gene expression. **f**, Percentage of cdGMP-Dy547$^+$ cells among cell populations in the TME following intratumoral administration of Dy547-cdGMP formulations ($n = 4$ biologically independent samples; one-way ANOVA with Tukey test). DC, dendritic cell; MΦ, macrophage; NK, natural killer cell; MDSC, myeloid-derived suppressor cell. **g**, Flow cytometric quantification of the MFI of cdGMP-Dy547$^+$ cells among the indicated cell populations in the TME ($n = 4$ biologically independent samples; two-way ANOVA with Sidak's multiple comparison test). **h**, *Ifnb1* expression following in vitro incubation with STING-NP, cGAMP or PBS for 4 h at doses equivalent to 150 nM cGAMP in RAW 264.7 macrophages, DC2.4 DCs, primary NK cells and B16.F10 melanoma cells ($n = 3$ biologically independent samples; one-way ANOVA with Tukey test). Significance levels are shown for comparisons between cells treated with STING-NP formulations. **i**, Fluorescence spectrophotometric quantification of cdGMP-dy547 accumulation in the sentinel lymph node 2 h following intratumoral administration (for cGAMP and STING-NP, $n = 3$ and 4 biologically independent samples, respectively; two-tailed Student's *t*-test). **j**, *Ifnb1* expression in the sentinel (inguinal) lymph node 4 h following intratumoral administration ($n = 3$ biologically independent samples; one-way ANOVA with Tukey test). Unless otherwise noted, statistical data are presented as means ± s.d.

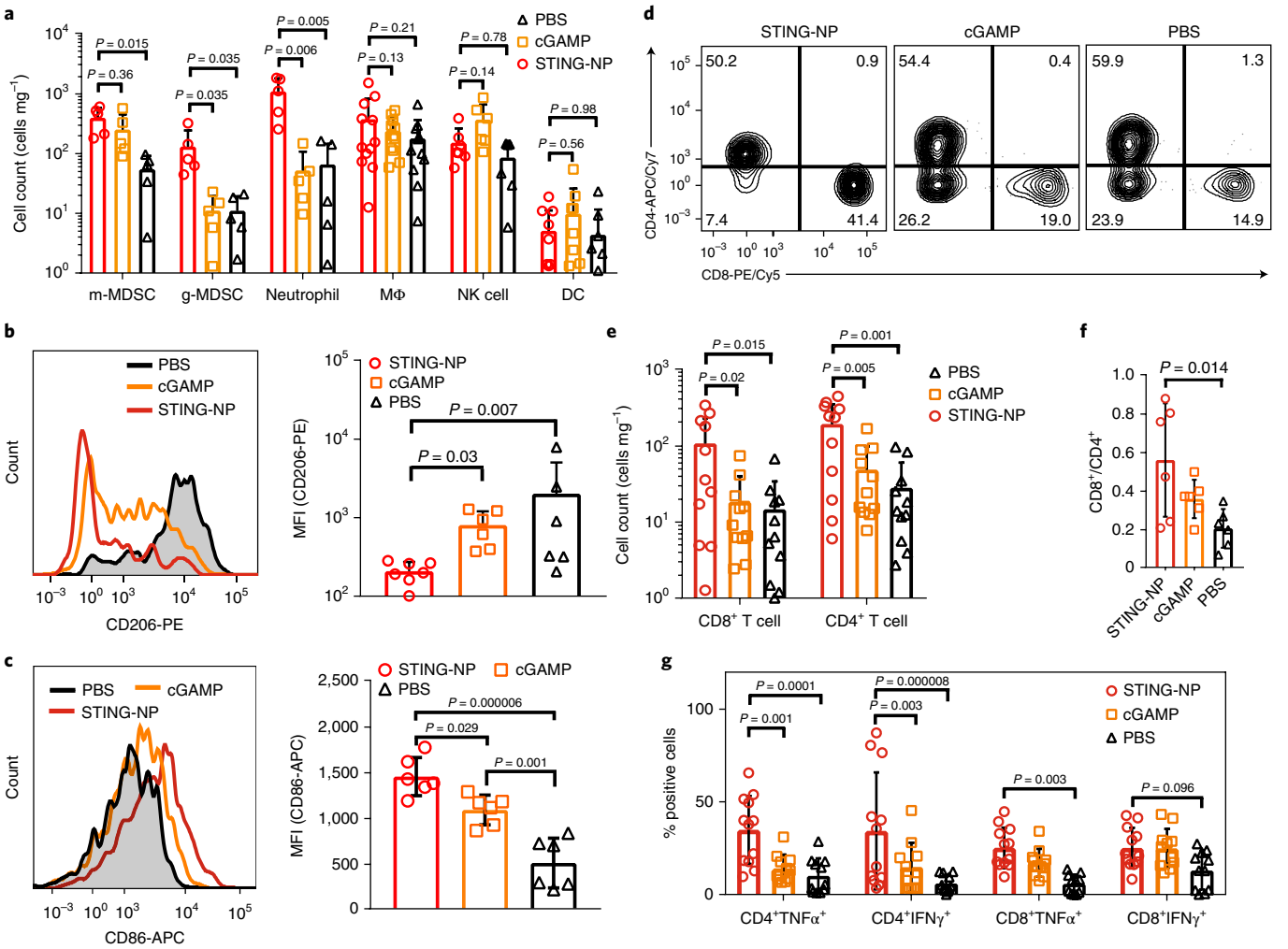

Fig. 3 | STING-NPs shift the immunocellular composition of the tumour microenvironment. a, Flow cytometric quantification of the number of monocytic (m-MDSC; CD11b$^+$Ly6c$^+$Ly6g$^-$) and granulocytic (g-MDSC; CD11b$^+$Ly6c$^+$Ly6g$^+$SSC^{hi}) MDSCs, activated neutrophils (CD11b$^+$Ly6c$^+$Ly6g$^+$SSC^{lo}), macrophages (MΦ; CD11b$^+$F4/80$^+$), natural killer cells (NK1.1$^+$) and dendritic cells (DCs; CD11c$^+$MHC-II$^+$) 48 h following intratumoral injection (n = 6, 6, 6, 11, 11 and 11 biologically independent samples, respectively; one-way ANOVA with Tukey test). **b**, Representative flow cytometry histogram (left) and quantification (right) of CD206 expression by intratumoral macrophages (n = 6 biologically independent samples; Kruskal–Wallace test with Dunn's multiple comparison test). **c**, Representative flow cytometry histogram (left) and quantification (right) of CD86 expressions by DCs in the inguinal lymph node (n = 6 biologically independent samples; one-way ANOVA with Tukey test). **d**,**e**, Representative flow cytometry dot plot (**d**) and quantification (**e**) of tumour-infiltrating CD4$^+$ and CD8$^+$ T cells 48 h following intratumoral injection (n = 11 biologically independent samples; one-way ANOVA with Tukey test). **f**, Ratio of CD8$^+$ to CD4$^+$ T cells in the TME (n = 11 biologically independent samples; one-way ANOVA with Tukey test). **g**, Intracellular cytokine staining and flow cytometry to evaluate TNF-α and IFN-γ production by tumour-infiltrating CD4$^+$ and CD8$^+$ T cells in response to PMA/ionomycin stimulation (n = 11 biologically independent samples; two-way ANOVA with Tukey test). Statistical data are represented as means ± s.d. All experiments were conducted twice independently with similar results.

route explored clinically (Fig. 4a–e)[51]. Using a poorly immunogenic B16.F10 melanoma model, we initiated treatment in mice with established (~14 d) and relatively large (111 ± 16 mm^3) subcutaneous tumours, which are more challenging to treat with immunotherapy than smaller tumours[52,53]. Treatment with STING-NPs resulted in an 11-fold decrease in the tumour growth rate (doubling time (DT)$_{STING\text{-}NP}$ = ~22.7 d) and significant increase in the survival time relative to cGAMP, which resulted in only a modest suppression of tumour growth (DT$_{cGAMP}$ = ~3.5 d; DT$_{PBS}$ = ~2.2 d) that did not confer a significant survival benefit (median survival (MS)$_{PBS}$ = 11 d; MS$_{cGAMP}$ = 12 d; MS$_{STING\text{-}NP}$ = 29 d). Treatment with empty particles did not affect tumour growth. Importantly, a physical mixture of cGAMP with pre-formulated empty vesicles yielded a nearly identical response to cGAMP, further corroborating in vitro data demonstrating the importance of encapsulating cGAMP into vesicles to achieve potent STING activation.

Approximately one-third of mice treated intratumorally with STING-NPs completely rejected tumours, without evidence of residual burden up to 65 d after tumour inoculation (Fig. 4e). We rechallenged these complete responders with B16.F10 tumour cells on the opposite flank and monitored the tumour volume. Without any additional treatment, five out of seven (~70%) rechallenged mice completely resisted tumour growth through at least 150 d. Tumour growth in the remaining two mice was also significantly slower relative to age-matched, treatment-naïve controls (Fig. 4f,g). To evaluate whether intratumoral injection of STING-NPs could suppress distal tumour growth, two subcutaneous B16.F10 tumours were concurrently established on contralateral flanks, and one tumour was

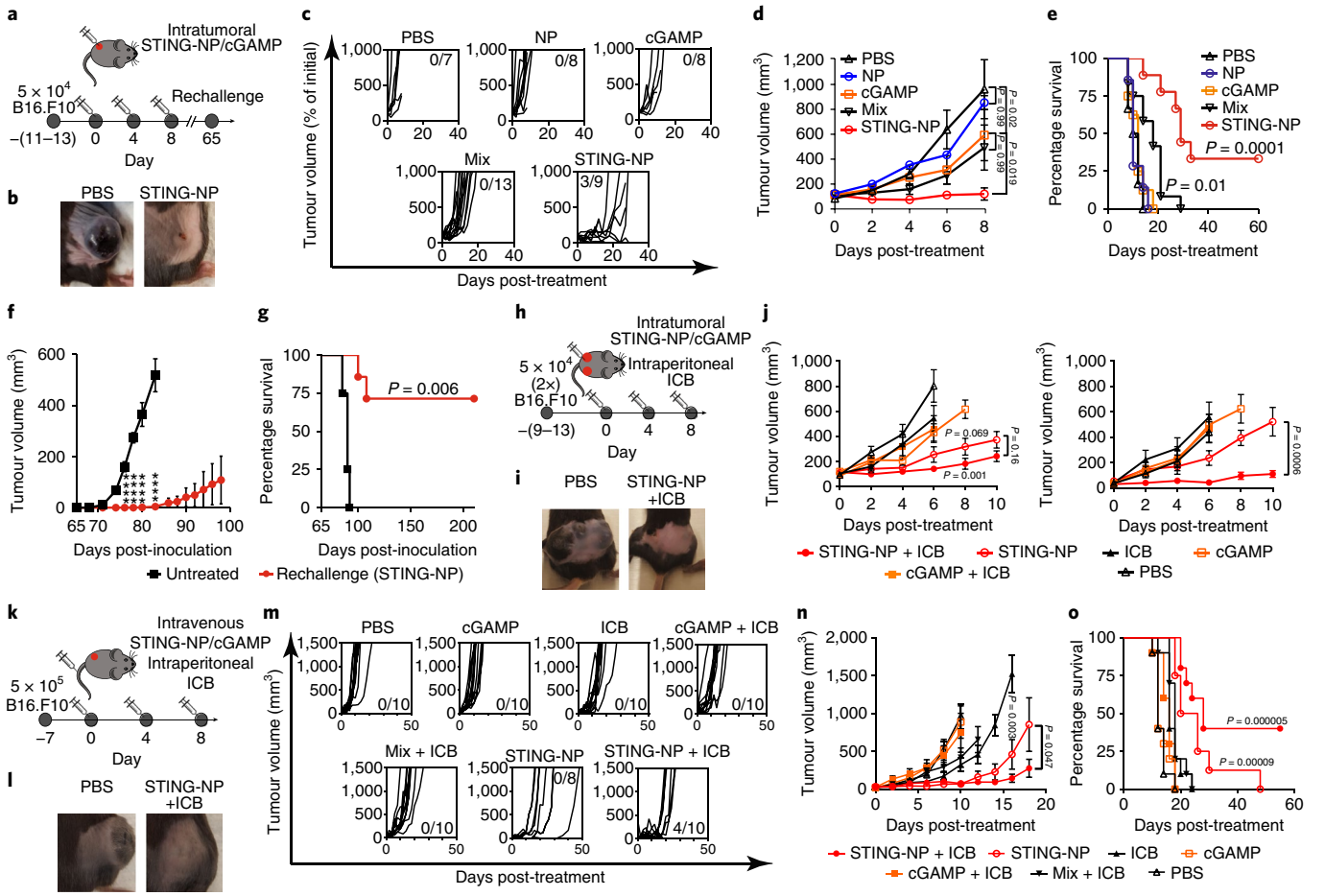

Fig. 4 | STING-NPs enhance the immunotherapeutic efficacy of cGAMP and synergize with ICB. a, Intratumoral administration and tumour rechallenge scheme for mice with a single established B16.F10 tumour. Mice with 100 mm^3 subcutaneous tumours were administered STING-NPs, free cGAMP, empty nanoparticles (NPs), a physical mixture of empty NPs and cGAMP (mix), or PBS intratumorally three times, 4 d apart. **b**, Photographs of tumours 8 d after treatment. The experiment was conducted three times independently with similar results. **c**, Spider plots of individual tumour growth curves, with the numbers of complete responses denoted. The experiment was conducted three times independently with similar results. **d**, Mean tumour volume from three independent experiments (for PBS, NP, cGAMP, mix and STING-NP; $n = 7$, 8, 8, 13 and 9 biologically independent samples, respectively; Kruskal–Wallis test with Dunn's multiple comparisons test). **e**, Kaplan–Meier survival curves of mice treated with the indicated formulation using a 1,500 mm^3 tumour volume as the endpoint criteria (for PBS, NP, cGAMP, mix and STING-NP, $n = 7$, 8, 8, 13 and 9 biologically independent samples, respectively; two-tailed Mantel–Cox test). **f**, Mice showing complete responses to STING-NP treatment were rechallenged with B16.F10 cells on the contralateral flank 65 d after inoculation without any further treatment (for treatment-naïve and rechallenged complete responses, $n = 4$ and 7 biologically independent samples; $^{****}P < 0.0001$, two-tailed Student's t-test). **g**, Kaplan–Meier survival curves for treatment-naïve and STING-NP-treated complete responses ($n = 7$; two-tailed Mantel–Cox test). **h**, Treatment scheme for mice with two concurrently established contralateral B16.F10 tumours. Mice were treated with the cGAMP-containing formulations intratumorally in one tumour and administered a combination of anti-PD-1 and anti-CTLA-4 antibodies (ICB) intraperitoneally three times, 4 d apart. **i**, Representative images of the tumours 8 d after initiation of STING-NP or PBS administration (injected into the left-flank tumour). The experiment was conducted twice independently with similar results. **j**, Average tumour volume of injected primary (left) and untreated contralateral (right) tumours (for PBS, cGAMP, ICB, cGAMP + ICB, STING-NP and STING-NP + ICB, $n = 11$, 7, 6, 10, 10 and 12 biologically independent samples, respectively; two-tailed Mann–Whitney U-test). $P = 0.069$ and $P = 0.001$ denote the significance levels of STING-NP- and STING-NP + ICB-treated mice, respectively, versus those treated with cGAMP (Kruskal–Wallis test with Dunn's multiple comparison test). **k**, Treatment scheme for mice treated intravenously with cGAMP formulations and intraperitoneally with ICB three times, 4 d apart. **l**, Representative images of tumours 8 d after initiation of treatment. The experiment was conducted three times independently with similar results. **m**, Spider plots of individual tumour growth curves of intravenously treated mice. **n**, Average tumour volume (two-tailed Mann–Whitney U-test; $P = 0.003$ denotes the significance of STING-NP relative to ICB). **o**, Kaplan–Meier survival analysis (two-tailed Mantel–Cox test). In **m**–**o**, for PBS, cGAMP, ICB, cGAMP + ICB, mix + ICB, STING-NP and STING-NP + ICB, $n = 10$, 10, 10, 10, 10, 8 and 10 biologically independent samples, respectively. All statistical data are represented as means ± s.e.m.

injected with STING-NP, cGAMP or PBS (Fig. 4h–j). STING-NP treatment significantly slowed the growth of the non-treated, contralateral tumour relative to PBS ($DT_{PBS} = \sim 1.9$ d; $DT_{STING\text{-}NP} = \sim 3.0$ d), although to a lesser extent than the treated tumour ($DT_{PBS} = \sim 1.7$ d; $DT_{STING\text{-}NP} = \sim 5.3$ d). Combining STING-NP treatment with systemic administration of anti-programmed death 1 (anti-PD-1) and anti-cytotoxic T-lymphocyte-associated antigen 4 (anti-CTLA-4) ICB further inhibited the growth of the untreated contralateral tumour ($DT_{STING\text{-}NP+ICB} = \sim 5.9$ d). (Fig. 4j). ICB (alone or in combination with free cGAMP) had no significant effect on the growth of either tumour.

While localized intratumoral delivery of STING agonists and other immunomodulators is emerging as a clinically viable treatment modality, this administration route may not be feasible for

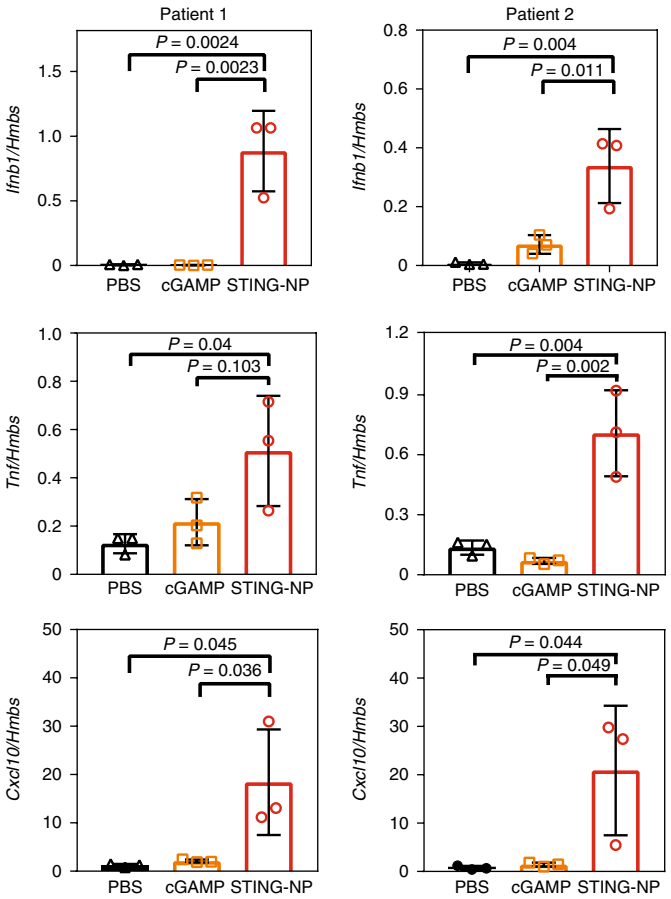

Fig. 5 | STING-NPs enhance cGAMP activity in human metastatic melanoma. Surgically resected melanoma metastases were divided into nine sections (three per treatment; one-way ANOVA with Tukey test), randomized, injected intratumorally with STING-NPs or cGAMP at 150 nM and cultured for 24 h. The graphs show the results of qPCR analysis of *Ifnb1*, *Tnf* and *Cxcl10* gene expression in tissues freshly isolated from two different melanoma patients after the indicated treatment. All statistical data are presented as means ± s.d.

many patients and/or cancer types, particularly in the setting of advanced, metastatic disease. We therefore evaluated the therapeutic efficacy of STING-NPs administered systemically via an intravenous route (Fig. 4k–o). Systemically administered STING-NP slowed subcutaneous tumour growth relative to free cGAMP, which demonstrated no therapeutic benefit (DT_{PBS} = ~1.9 d; DT_{cGAMP} = ~1.9 d; $DT_{STING\text{-}NP}$ = ~3.8 d) even when combined with ICB ($DT_{cGAMP+ICB}$ = ~2.8 d). In contrast, systemic STING-NP significantly improved the response to anti-PD-1 + anti-CTLA-4 ICB ($DT_{STING\text{-}NP+ICB}$ = ~5.0 d). Improved responses to ICB were not observed using a mixture of empty nanoparticles and free cGAMP. A mild acute decrease in body weight was observed following intravenous administration of STING-NPs, followed by full weight recovery without elevation in serum levels of alanine aminotransferase, bilirubin or creatinine over mice administered PBS. Additionally, histological analysis revealed no evidence of liver damage due to the administration of STING-NPs (Supplementary Fig. 9). Importantly, 40% of mice (4 out of 10) administered STING-NPs systemically in combination with ICB exhibited complete responses, with no evidence of tumour burden for at least 55 d after the cessation of therapy (Fig. 4o). This shows that intravenously administered CDN STING agonists can confer a significant survival benefit while synergizing with ICB to yield complete and durable responses, offering an opportunity to utilize STING agonists in patients with non-accessible tumours.

To support the translational potential of STING-NPs, we directly injected freshly resected human metastatic melanoma tissue specimens with STING-NP, cGAMP or PBS, and quantified *Ifnb1*, *Tnfa* and *Cxcl10* levels via qPCR (Fig. 5). Consistent with the findings in murine models, STING-NPs demonstrated superior immunostimulatory activity, increasing the expression of *Ifnb1* (48–352-fold) and *Tnf* (4–5-fold), as well as *Cxcl10* (15–23-fold)—a chemokine that correlates with T-cell infiltration in human metastatic melanoma[41]. This effect was consistent in tumours from two different melanoma patients, supporting the potential use of STING-NPs as a strategy to increase the immunogenicity of human tumours.

Conclusions

Through the rational design of nanoparticle properties, we have designed endosomolytic polymersomes to enhance the cytosolic delivery of cGAMP. Owing to both their nanoscale properties and immunostimulatory activity, STING-NPs provide advantages over existing STING agonists and CDN delivery technologies in terms of: (1) the superior activation of the STING pathway; (2) the ability to enhance STING activation in both the tumour and sentinel lymph node; (3) the therapeutic efficacy achieved through both intravenous and intratumoral administration routes; and (4) the enhanced synergy with ICB. In doing so, this work also elucidated important relationships between polymer structure, colloidal self-assembly and CDN delivery, highlighting key distinctions between the delivery of nucleic acid therapeutics and CDNs while establishing new design principles for the nanoparticle delivery of STING agonists. Our findings indicate that STING-NPs enhance the cytosolic delivery of cGAMP via an endosomal escape mechanism, preferentially activating STING in myeloid cell populations within the TME and TDLN to trigger a multifaceted shift to a 'hot' T-cell-inflamed TME that inhibits tumour growth. As a single agent, locally administered STING-NPs can generate robust and complete responses, eliciting systemic antitumour immunity that can protect against tumour rechallenge. Importantly, STING-NPs can be administered through both intratumoral and intravenous routes, either as monotherapy or in combination with ICB for therapeutic benefit, potentially opening new clinical opportunities for leveraging STING agonists. Therefore, STING-NPs represent a significant technological advancement with the potential to expand the immunotherapeutic armamentarium.

Online content

Any methods, additional references, Nature Research reporting summaries, source data, statements of data availability and associated accession codes are available at https://doi.org/10.1038/s41565-018-0342-5.

Received: 12 July 2018; Accepted: 26 November 2018;
Published online: 21 January 2019

References

1. Ribas, A. & Wolchok, J. D. Cancer immunotherapy using checkpoint blockade. *Science* **359**, 1350–1355 (2018).
2. Sharma, P. & Allison, J. P. The future of immune checkpoint therapy. *Science* **348**, 56–61 (2015).
3. Vanpouille-Box, C. et al. Trial watch: immune checkpoint blockers for cancer therapy. *Oncoimmunology* **6**, e1373237 (2017).
4. Khalil, D. N., Smith, E. L., Brentjens, R. J. & Wolchok, J. D. The future of cancer treatment: immunomodulation, CARs and combination immunotherapy. *Nat. Rev. Clin. Oncol.* **13**, 273–290 (2016).
5. Gotwals, P. et al. Prospects for combining targeted and conventional cancer therapy with immunotherapy. *Nat. Rev. Cancer* **17**, 286–301 (2017).
6. Binnewies, M. et al. Understanding the tumor immune microenvironment (TIME) for effective therapy. *Nat. Med.* **24**, 541–550 (2018).

7. Chen, D. S. & Mellman, I. Elements of cancer immunity and the cancer-immune set point. *Nature* **541**, 321–330 (2017).
8. Fridman, W. H., Zitvogel, L., Sautes-Fridman, C. & Kroemer, G. The immune contexture in cancer prognosis and treatment. *Nat. Rev. Clin. Oncol.* **14**, 717–734 (2017).
9. Woo, S. R. et al. STING-dependent cytosolic DNA sensing mediates innate immune recognition of immunogenic tumors. *Immunity* **41**, 830–842 (2014).
10. Deng, L. et al. STING-dependent cytosolic DNA sensing promotes radiation-induced type I interferon-dependent antitumor immunity in immunogenic tumors. *Immunity* **41**, 843–852 (2014).
11. Gao, P. et al. Cyclic [G(2′,5′)pA(3′,5′)p] is the metazoan second messenger produced by DNA-activated cyclic GMP-AMP synthase. *Cell* **153**, 1094–1107 (2013).
12. Diner, E. J. et al. The innate immune DNA sensor cGAS produces a noncanonical cyclic dinucleotide that activates human STING. *Cell Rep.* **3**, 1355–1361 (2013).
13. Ablasser, A. et al. cGAS produces a 2′-5′-linked cyclic dinucleotide second messenger that activates STING. *Nature* **498**, 380–384 (2013).
14. Zhang, X. et al. Cyclic GMP-AMP containing mixed phosphodiester linkages is an endogenous high-affinity ligand for STING. *Mol. Cell* **51**, 226–235 (2013).
15. Gao, P. et al. Structure–function analysis of STING activation by c[G(2′,5′) pA(3′,5′)p] and targeting by antiviral DMXAA. *Cell* **154**, 748–762 (2013).
16. Chen, Q., Sun, L. & Chen, Z. J. Regulation and function of the cGAS–STING pathway of cytosolic DNA sensing. *Nat. Immunol.* **17**, 1142–1149 (2016).
17. Corrales, L., McWhirter, S. M., Dubensky, T. W. Jr & Gajewski, T. F. The host STING pathway at the interface of cancer and immunity. *J. Clin. Invest.* **126**, 2404–2411 (2016).
18. Wang, H. et al. cGAS is essential for the antitumor effect of immune checkpoint blockade. *Proc. Natl Acad. Sci. USA* **114**, 1637–1642 (2017).
19. Ishikawa, H., Ma, Z. & Barber, G. N. STING regulates intracellular DNA-mediated, type I interferon-dependent innate immunity. *Nature* **461**, 788–792 (2009).
20. Corrales, L. et al. Direct activation of STING in the tumor microenvironment leads to potent and systemic tumor regression and immunity. *Cell Rep.* **11**, 1018–1030 (2015).
21. Demaria, O. et al. STING activation of tumor endothelial cells initiates spontaneous and therapeutic antitumor immunity. *Proc. Natl Acad. Sci. USA* **112**, 15408–15413 (2015).
22. Ohkuri, T. et al. Intratumoral administration of cGAMP transiently accumulates potent macrophages for anti-tumor immunity at a mouse tumor site. *Cancer Immunol. Immunother.* **66**, 705–716 (2017).
23. Curran, E. et al. STING pathway activation stimulates potent immunity against acute myeloid leukemia. *Cell Rep.* **15**, 2357–2366 (2016).
24. Fu, J. et al. STING agonist formulated cancer vaccines can cure established tumors resistant to PD-1 blockade. *Sci. Transl. Med.* **7**, 283ra252 (2015).
25. Dubensky, T. W. Jr., Kanne, D. B. & Leong, M. L. Rationale, progress and development of vaccines utilizing STING-activating cyclic dinucleotide adjuvants. *Ther. Adv. Vaccines* **1**, 131–143 (2013).
26. Koshy, S. T., Cheung, A. S., Gu, L., Graveline, A. R. & Mooney, D. J. Liposomal delivery enhances immune activation by STING agonists for cancer immunotherapy. *Adv. Biosyst.* **1**, 1600013 (2017).
27. Hanson, M. C. et al. Nanoparticulate STING agonists are potent lymph node-targeted vaccine adjuvants. *J. Clin. Invest.* **125**, 2532–2546 (2015).
28. Mullard, A. Can innate immune system targets turn up the heat on 'cold' tumours? *Nat. Rev. Drug Discov.* **17**, 3–5 (2018).
29. Vrignaud, S., Benoit, J. P. & Saulnier, P. Strategies for the nanoencapsulation of hydrophilic molecules in polymer-based nanoparticles. *Biomaterials* **32**, 8593–8604 (2011).
30. Manganiello, M. J., Cheng, C., Convertine, A. J., Bryers, J. D. & Stayton, P. S. Diblock copolymers with tunable pH transitions for gene delivery. *Biomaterials* **33**, 2301–2309 (2012).
31. Wilson, J. T. et al. Enhancement of MHC-I antigen presentation via architectural control of pH-responsive, endosomolytic polymer nanoparticles. *AAPS. J.* **17**, 358–369 (2014).
32. O'Neil, C. P., Suzuki, T., Demurtas, D., Finka, A. & Hubbell, J. A. A novel method for the encapsulation of biomolecules into polymersomes via direct hydration. *Langmuir* **25**, 9025–9029 (2009).
33. Kilchrist, K. V., Evans, B. C., Brophy, C. M. & Duvall, C. L. Mechanism of enhanced cellular uptake and cytosolic retention of MK2 inhibitory peptide nano-polyplexes. *Cell Mol. Bioeng.* **9**, 368–381 (2016).
34. Nelson, C. E. et al. Balancing cationic and hydrophobic content of PEGylated siRNA polyplexes enhances endosome escape, stability, blood circulation time, and bioactivity in vivo. *ACS Nano* **7**, 8870–8880 (2013).
35. Discher, D. E. & Ahmed, F. Polymersomes. *Annu. Rev. Biomed. Eng.* **8**, 323–341 (2006).
36. Jain, S. & Bates, F. S. Consequences of nonergodicity in aqueous binary PEO–PB micellar dispersions. *Macromolecules* **2004**, 1511–1523 (2004).
37. Mai, Y. & Eisenberg, A. Self-assembly of block copolymers. *Chem. Soc. Rev.* **41**, 5969–5985 (2012).
38. Parker, B. S., Rautela, J. & Hertzog, P. J. Antitumour actions of interferons: implications for cancer therapy. *Nat. Rev. Cancer* **16**, 131–144 (2016).
39. Yin, H. et al. Non-viral vectors for gene-based therapy. *Nat. Rev. Genet.* **15**, 541–555 (2014).
40. Wilson, D. R. et al. Biodegradable STING agonist nanoparticles for enhanced cancer immunotherapy. *Nanomedicine* **14**, 237–246 (2018).
41. Harlin, H. et al. Chemokine expression in melanoma metastases associated with $CD8^+$ T-cell recruitment. *Cancer Res.* **69**, 3077–3085 (2009).
42. Munn, D. H. & Mellor, A. L. The tumor-draining lymph node as an immune-privileged site. *Immunol. Rev.* **213**, 146–158 (2006).
43. Reddy, S. T., Rehor, A., Schmoekel, H. G., Hubbell, J. A. & Swartz, M. A. In vivo targeting of dendritic cells in lymph nodes with poly(propylene sulfide) nanoparticles. *J. Control. Release* **112**, 26–34 (2006).
44. Reddy, S. T. et al. Exploiting lymphatic transport and complement activation in nanoparticle vaccines. *Nat. Biotechnol.* **25**, 1159–1164 (2007).
45. Lizotte, P. H. et al. In situ vaccination with cowpea mosaic virus nanoparticles suppresses metastatic cancer. *Nat. Nanotechnol.* **11**, 295–303 (2016).
46. Mantovani, A., Cassatella, M. A., Costantini, C. & Jaillon, S. Neutrophils in the activation and regulation of innate and adaptive immunity. *Nat. Rev. Immunol.* **11**, 519–531 (2011).
47. Liang, H. et al. Host STING-dependent MDSC mobilization drives extrinsic radiation resistance. *Nat. Commun.* **8**, 1736 (2017).
48. Shi, L. et al. PD-1 blockade boosts radiofrequency ablation-elicited adaptive immune responses against tumor. *Clin. Cancer Res.* **22**, 1173–1184 (2016).
49. Ries, C. H. et al. Targeting tumor-associated macrophages with anti-CSF-1R antibody reveals a strategy for cancer therapy. *Cancer Cell* **25**, 846–859 (2014).
50. Rudqvist, N. P. et al. Radiotherapy and CTLA-4 blockade shape the TCR repertoire of tumor-infiltrating T cells. *Cancer Immunol. Res.* **6**, 139–150 (2018).
51. Murthy, V., Minehart, J. & Sterman, D. H. Local immunotherapy of cancer: innovative approaches to harnessing tumor-specific immune responses. *J. Natl Cancer Inst.* **109**, djx097 (2017).
52. Overwijk, W. W. et al. Tumor regression and autoimmunity after reversal of a functionally tolerant state of self-reactive $CD8^+$ T cells. *J. Exp. Med.* **198**, 569–580 (2003).
53. Moynihan, K. D. et al. Eradication of large established tumors in mice by combination immunotherapy that engages innate and adaptive immune responses. *Nat. Med.* **22**, 1402–1410 (2016).

Acknowledgements

We thank K. Rock for providing the DC2.4 cells, C. Duvall for use of the gel permeation chromatography equipment and in vivo imaging system, A. Richmond and A. Vilgelm for consultation on flow cytometry protocols, and J. Rhoades and A. Merkel for technical advice on tumour models. We thank the Koch Institute Swanson Biotechnology Center (specifically the Nanotechnology Materials Core Facility) for technical support on the cryogenic electron microscopy, the core facilities of the Vanderbilt Institute of Nanoscale Science and Engineering for use of dynamic light scattering and transmission electron microscope instruments, the VUMC Flow Cytometry Shared Resource (supported by the Vanderbilt-Ingram Cancer Center (VICC) (P30 CA68485) and Vanderbilt Digestive Disease Research Center (DK058404)) for the use of BD three-laser LSRII and BD five-laser LSRFortessa flow cytometers, the Vanderbilt Translational Pathology Shared Resource (supported in part by NCI/NIH Cancer Center Support Grant 5P30 CA684850-19) and the Vanderbilt Technologies for Advanced Genomics. 2′3′-cGAMP was provided by the Vanderbilt Institute of Chemical Biology Chemical Synthesis Core. This research was supported by grants from the National Science Foundation (1554623 to J.T.W.), Alex's Lemonade Stand Foundation (SID924 to J.T.W.), the National Institutes of Health (K23 CA204726/CA/NCI to D.B.J., R00CA181491 to J.M.B. and 5R35GM119569-03 to M.A.), the VICC (Support Grant P30 CA68485 and VICC Ambassador Discovery Grant to M.A., and VICC-Vanderbilt Center for Immunobiology Pilot Grant to J.T.W.), the Melanoma Research Alliance (503565 to J.T.W.) and Stand Up To Cancer (SU2C) (Innovative Research Grant, grant no. SU2C-AACR-IRG 20-17 to J.T.W.). SU2C is a division of the Entertainment Industry Foundation. Research grants are administered by the American Association for Cancer Research, the scientific partner of SU2C.

Author contributions

D.S. and J.T.W. conceived of and designed the experiments. D.S. performed the majority of the experiments and data analysis. K.W.B. created the ISRE luciferase reporter B16. F10 cells used for longitudinal in vivo experimentation and assisted with tumour therapy studies. P.C. synthesized and characterized 2′3′-cGAMP. D.S.Y. and A.K.R.L.-J.

obtained cryogenic transmission electron micrographs of nanoparticles. S.S. synthesized and characterized the PDSMA monomer. M.A. assisted with experimental design and cGAMP characterization. M.K. and D.B.J. provided resected tumour samples from melanoma patients. J.M.B. provided guidance on, and assisted with, the NanoString experiments and analysis of multiplexed gene expression data. D.S. and J.T.W. wrote the manuscript.

Competing interests

J.T.W. and D.S. are inventors on a pending patent related to the technology described in this manuscript. D.B.J. serves on the advisory board for Bristol-Myers Squibb and Merck, and receives research support from Bristol-Myers Squibb that is unrelated to this manuscript. J.M.B. receives research funding from Bristol-Myers Squibb, Genentech and Incyte, receives consulting and expertise testimony compensation from Novartis, and has patents pending concerning the use of HLA-DR as a predictive marker in immunotherapy responses.

Additional information

Supplementary information is available for this paper at https://doi.org/10.1038/s41565-018-0342-5.

Reprints and permissions information is available at www.nature.com/reprints.

Correspondence and requests for materials should be addressed to J.T.W.

Publisher's note: Springer Nature remains neutral with regard to jurisdictional claims in published maps and institutional affiliations.

© The Author(s), under exclusive licence to Springer Nature Limited 2019

Methods

Synthesis and characterization of block copolymers. BMA, poly(ethylene glycol) 4-cyano-4-(phenylcarbonothioylthio)pentanoate (PEG-CPADB; $M_n = 2{,}000$ and 10,000 Da), 4-cyano-4-(phenylcarbonothioylthio)pentanoate (CPADB), *N*,*N*′-dicyclohexylcarbodiimide, 4-(dimethylamino)pyridine, DTT, 4,4′-azobis(4-cyanovaleric acid) (V501), dichloromethane, 1,4-dioxane and poly(ethylene glycol) methyl ether ($M_n = 5{,}000$ Da) were purchased from Sigma–Aldrich. 2-(Diethylamino)ethyl methacrylate (DEAEMA) was procured from TCI Chemicals, and 2,2′-azobis(4-methoxy-2,4-dimethylvaleronitrile) (V70) was purchased from Wako Chemicals. PDSMA was synthesized according to a previously reported procedure[54]. Butylated hydroxytoluene inhibitor was removed from methacrylate monomers before further use by gravity chromatography using basic alumina (Sigma).

For the synthesis of the PEG-DB polymers, the appropriate PEG-CPADB macro-RAFT chain transfer agent (mCTA) was dissolved in anhydrous dioxane with purified BMA, DEAEMA and V501 at a 60:40 molar ratio of BMA:DEAEMA, sealed with septa, purged with N_2 for 20 min and polymerized at 70 °C for 18 h. An initiator-to-mCTA ratio of 0.2:1 was used with a combined monomer and mCTA-to-dioxane weight ratio of 0.4. Polymers were precipitated twice in cold pentane and vacuum dried. Polymer compositions were characterized via ^{1}H-NMR in $CDCl_3$ on a Bruker AV400 spectrometer (Supplementary Fig. 10). The molecular weight and polydispersity index were quantified using gel permeation chromatography (Agilent) with dimethylformamide containing 0.1 M LiBr as the mobile phase, and in-line light scattering (Wyatt) and refractive index (Agilent) detectors. PEG_{5kDa}-CPADB or PEG_{10kDa}-CPADB mCTAs were synthesized as previously described[55]. PEG_{2kDa}-$DBP_{4.5kDa}$ was synthesized under similar conditions, using a 55:37:8 molar ratio of DEAEMA:BMA:PDSMA, substituting V70 for V501, and at a reaction temperature of 30 °C for 24 h.

Synthesis of 2′3′-cGAMP. 2′3′-cGAMP was synthesized using a method adapted from Gaffney et al.[56] (Supplementary Scheme 1). Adenosine phosphoramidite (1 g, 1 mmol) was dissolved in 7 ml of acetonitrile (ACN) and water (0.036 ml, 2 mmol). Pyridinium trifluoroacetate (0.231 g, 1.2 mmol) was added and the reaction mixture was stirred for 1 min. *tert*-Butylamine (8 ml) was added, and the reaction mixture was stirred for 10 min at room temperature. Solvent was removed by rotary evaporation to yield a gummy residue that was dissolved in 15 ml of dichloromethane (DCM). Sequentially, water (0.18 ml, 10 mmol) and dichloroacetic acid (27 ml, 3% in DCM, 10 mmol) were added and the reaction mixture was stirred at room temperature for 10 min. Pyridine (1.6 ml, 20 mmol) was added and the solvent was removed by rotary evaporation. The residue was dissolved in 10 ml of ACN and concentrated. This process was repeated three times. The oily product was dissolved in anhydrous ACN (3 ml), and a solution of guanosine phosphoramidite (1.27 g, 1.2 mmol, dissolved in 3 ml of anhydrous ACN) was added. The guanosine phosphoramidite was co-evaporated with anhydrous ACN (3 × 20 ml) and vacuum dried overnight. After stirring for 2 min, anhydrous *tert*-butyl hydroperoxide (5.5 M in decane, 0.55 ml, 3 mmol) was added, and the reaction mixture was additionally stirred for 30 min at room temperature. $NaHSO_3$ (0.3 g, dissolved in 0.8 ml water) was added and the mixture was stirred for 5 min. The solvent was removed by rotary evaporation. The oily product was dissolved in DCM (18 ml), and water (0.18 ml, 10 mmol) and dichloroacetic acid (27 ml, 3% in DCM, 10 mmol). The reaction mixture was stirred for 10 min at room temperature and quenched with pyridine (10 ml). The solvent was removed by rotary evaporation and the residue was co-evaporated with anhydrous pyridine (2 × 10 ml). The oily residue was dissolved in anhydrous pyridine (17 ml), and 5,5-dimethyl-2-oxo-2-chloro-1,3,2-dioxaphosphinane (0.65 g, 3.5 mmol) was added. The reaction mixture was stirred at room temperature for 10 min, then water (0.63 ml, 35 mmol) and iodine (0.330 g, 1.3 mmol) were added sequentially. After stirring for 5 min, the reaction mixture was poured into a solution of $NaHSO_3$ (0.2 g in 150 ml of water). Solid $NaHCO_3$ (4 g) was slowly added after 5 min and the stirring was continued for 5 min. The water was transferred into a separatory funnel and a mixture of ethyl acetate and diethyl ether was added (150 ml, 1:1). The organic layer was separated and the aqueous layer was extracted with an additional mixture of ethyl acetate and diethyl ether (80 ml, 1:1). The organic layers were combined and concentrated to an oil. The residue was purified by flash chromatography (CombiFlash Rf, DCM/methanol = 0–25% for 20 min) to give a solid. The solid was dissolved in CH_3NH_2 in anhydrous ethanol (33% by weight, 24 ml, 212 mmol). The reaction mixture was stirred at room temperature for 4 h. The solvent was removed by rotary evaporation to give a solid. The solid was co-evaporated with a mixture of anhydrous pyridine and triethyl amine (four times, 5 ml, 4:1) to give an oily product. The oily product was dissolved in anhydrous pyridine (2 ml), and triethyl amine (8 ml) and $Et3N_x3HF$ (3.3 ml, 60 mmol fluorine, 30 equivalence relative to each tert-butyldimethylsilyl ether) were added simultaneously. The reaction mixture was stirred at 55 °C for 3 h. After the reaction mixture was cooled down, acetone (high-performance liquid chromatography grade, 80 ml) was slowly added. The precipitate was filtered off and washed with acetone (5 × 5 ml). The final compound was purified on a Gemini–NX C18 column (250 × 10 mm^2, flow rate: 5 ml min^{-1} with ultraviolet detection at 254 nm) using a gradient of 1–5% for 20 min (CH_3CN in 0.1 M NH_4HCO_3). ^{1}H-NMR spectra (Supplementary Fig. 11) and liquid chromatography–mass spectrometry data (Supplementary Fig. 12) of purified 2′3′-cGAMP are provided in the Supplementary Information. The biological activity of synthesized 2′3′-cGAMP (both free and incorporated into STING-NPs) was validated by comparison with a commercial source (2′3-cGAMP VacciGrade; InvivoGen; Supplementary Fig. 13).

Polymer self-assembly and particle characterization. Block copolymers were mixed with ethanol to a concentration of 1,250 mg ml^{-1} and allowed to equilibrate for at least 20 min in a 2 ml microfuge tube at 37 °C. A 1× volume equivalent of deionized water containing the encapsulant (50 mg ml^{-1} cGAMP) was added to the polymer mixture, followed by centrifugation at 2,000*g* for 2 min. The mixture was allowed to equilibrate for 20 min before a 3× volume of 25% ethanol in water was added to the mixture and centrifuged again for 2 min. Then, a 7.5× volume equivalent of water was added to the mixture, which was briefly vortexed and sonicated at 40 °C until the polymer was completely dispersed into colloidal suspension. For the crosslinked PEG-DBP particles, the particle suspension was diluted to 1 ml and crosslinked through the addition of aqueous DTT. To purify and concentrate the particles, the sample was diluted to 15 ml in deionized water, followed by centrifugal dialysis, twice (Amicon; 10 kDa molecular weight cut-off). For cGAMP-loaded particles, an aliquot was removed, added to 9 volumes of pH 5.8 PBS and analysed by high-performance liquid chromatography with an isocratic mobile phase of water with 0.1% trifluoroacetic acid to determine the cGAMP concentration.

To measure the particle size distribution and zeta potential, particles were diluted in 10 mM PBS of the appropriate pH and characterized using a Malvern Nano ZS. For transmission electron microscopy, particles were drop cast onto an ultrathin carbon/lacey support grid (Ted Pella), stained with a 2% solution of methylamine tungstate for 30 s and imaged on a 200 kV Osiris Transmission Electron Microscope.

Cryogenic TEM samples were prepared on a Gatan Cryoplunge III. Some 3 µl of sample (at 1 mg ml^{-1}) was dropped on a lacey copper grid coated with a continuous carbon film. The Cryoplunge III blotter was used to remove excess sample without damaging the carbon layer before plunge freezing. The frozen grid was mounted on a Gatan 626 single-tilt cryo-transfer holder, and a transfer workstation with liquid nitrogen was used to maintain the specimen and holder under frozen conditions before imaging. The sample was imaged on a JEOL 2100 field emission electron gun. The microscope was operated at 200 kV. All images were recorded on a Gatan UltraScan charge-coupled device camera.

Red blood haemolysis assay. De-identified human whole blood was acquired from Vanderbilt Technologies for Advanced Genomics. Erythrocytes were pelleted at 500 r.c.f. and washed three times with PBS. Following the third wash, the erythrocytes were suspended in 100 mM PBS of the desired pH and plated in a 96-well V-bottom plate. The erythrocytes were treated with nanoparticles at a concentration of 10 µg ml^{-1} at 37 °C for 1 h. The plates were then centrifuged at 700 r.c.f., and the supernatant was transferred to a 96-well flat-bottom plate for quantification of the haemoglobin leakage via absorbance spectroscopy ($\lambda = 575$ nm).

Cell culture. The DC2.4 cells were kindly provided by K. Rock (University of Massachusetts Medical School) and cultured in Roswell Park Memorial Institute (RPMI) 1640 Medium (Gibco) supplemented with 10% foetal bovine serum (FBS; Gibco), 100 U ml^{-1} penicillin (Gibco), 100 µg ml^{-1} streptomycin (Gibco), 2 mM L-glutamine, 50 µM 2-mercaptoethanol (Gibco), 1× non-essential amino acids (Cellgro) and 10 mM HEPES (Invitrogen). B16-Blue ISG, THP1-Blue ISG and RAW-Blue ISG cells were purchased from InvivoGen and cultured according to the manufacturer's specifications. No authentication of the cell lines was performed by the authors. All cells lines were tested for *Mycoplasma* contamination and grown in a humidified atmosphere with 5% CO_2 at 37 °C.

In vitro evaluation of CDN activity and cellular uptake. THP1 ISG, DC2.4, B16 ISG and RAW-Blue ISG cell lines were plated at densities of 10,000, 10,000, 50,000 and 50,000 cells well^{-1}, respectively, in a 96-well plate. Cells were treated with the indicated formulations for 24 h. For ISG reporter cell lines, the relative expression of ISRE genes was examined using the QUANTI-Blue reagent (InvivoGen). For dendritic cells, secreted IFN-β was quantified with the LumiKine Xpress mIFN-β enzyme-linked immunosorbent assay kit (InvivoGen).

To quantify the relative cellular CDN uptake, B16.F10, RAW 264.7, DC2.4 and primary murine natural killer cells were seeded at 100,000 cells well^{-1} in 12-well plates and treated with co-formulations of cdGMP-Dy547 (Axxora) and cGAMP for 2 h at concentrations of 2 and 100 ng ml^{-1}, respectively. Natural killer cells were isolated from the spleens of 6–8-week-old female C57BL6/J mice. The spleens were mechanically dissociated, strained through a 40 µm cell strainer and enriched for natural killer cells through an EasySep Mouse NK Cell Isolation Kit (STEMCELL Technologies). After incubation for 2 h, the cells were suspended in a 2% bovine serum albumin in PBS solution and analysed via flow cytometry using a 561 nm excitation laser and 582/15 filter configuration on a BD LSRFortessa.

Mouse care and experimentation. Female C57BL/6 mice (6–8 weeks old) were purchased from The Jackson Laboratory. All animals were maintained at the

animal facilities of Vanderbilt University under specific pathogen-free conditions and treated in accordance with the regulations and guidelines of the Institutional Animal Care and Use Committee. All animal experiments were approved by the Vanderbilt University Institutional Animal Care and Use Committee.

In vivo imaging system imaging. B16.F10 melanoma cells were transduced to express luciferase in an ISRE-dependent manner via the Cignal Lenti Reporter construct (Qiagen). Transduced cells were grown and expanded in medium containing the selection agent puromycin at a concentration of 10 μg ml^{-1}. Transduction was verified by treating the cells with mouse IFN-β and monitoring the luciferase production.

5×10^4 B16.F10 cells containing the reporter construct were injected subcutaneously into the flank of 6–8-week-old female C57BL/6 mice (The Jackson Laboratory). On reaching ~100 mm^3, the tumours were injected intratumorally with 100 μl PBS containing 10 μg cGAMP in the appropriate formulation. Mice were injected intraperitoneally with 200 μl of 15 mg ml^{-1} D-luciferin (Thermo Fisher Scientific) in PBS. Fifteen minutes following injection, luminescence was quantified on the IVIS Lumina III (PerkinElmer) using Living Image software (version 4.5, http://www.perkinelmer.com/category/in-vivo-imaging-software).

Gene expression analysis following intratumoral administration. Female C57BL/6J mice aged 6–8 weeks were inoculated subcutaneously with 50,000 B16.F10 cells. On reaching an average size of ~100 mm^3, the tumours were treated via intratumoral injection with 100 μl of either PBS, free cGAMP or STING-NP nanoparticle formulations (10 μg cGAMP per injection). For qPCR analysis, tumours were harvested after 4 h and lysed in RLT lysis buffer (Qiagen) supplemented with 2% β-mercaptoethanol (Sigma) in a gentleMACS M tube with mechanical disruption using an OctoMACS tissue dissociator (Miltenyi). Tumour RNA was isolated with an RNeasy RNA isolation kit (Qiagen) with the RNase-free DNase Set (Qiagen), used according to manufacturer's specifications. Complementary DNA (cDNA) was synthesized with the Bio-Rad iScript cDNA kit and analysed via qPCR using the appropriate TaqMan kits (Thermo Fisher Scientific). The TaqMan gene expression kits were: Mm00443258_m1 for mouse *Tnf*; Mm00439552_s1 for mouse *Ifnb1*; Mm00434946_m1 for mouse *Cxcl9*; Mm00445235_m1 for mouse *Cxcl10*; and Mm01143545_m1 for mouse *Hmbs*.

Quantification of CDN accumulation and *Ifnb1* expression in the TDLN. Subcutaneous B16.F10 tumours of ~100 mm^3 were injected with co-formulations of cGAMP (10 μg) and cdGMP-Dy547 (0.2 μg). Then, 1 h after injection, the mice were euthanized and the inguinal TDLN was harvested, placed in RLT tissue lysis buffer (Qiagen) and homogenized using an OctoMACS tissue dissociator. cdGMP-Dy547 was quantified in the resulting lysate on a Synergy H1 plate reader (576/550 excitation/emission). Background fluorescence was removed by subtracting baseline fluorescence values of TDLN lysates from PBS-treated tumour-bearing mice. For quantification of *Ifnb1* expression, subcutaneous B16.F10 tumours were injected with cGAMP formulations (10 μg). TDLNs were harvested 2 h after injection. Messenger RNA isolation, cDNA synthesis and qPCR quantification of *Ifnb1* transcription were performed as described above.

NanoString nCounter analysis. From the tumour samples, 100 ng of RNA was isolated, as previously described, 4 h after treatment and analysed by NanoString nCounter gene expression analysis using the PanCancer Immune Profiling Panel. The fold change was calculated by comparing against the average normalized gene expression values of PBS-treated tumours. All statistical significance and clustering analysis was performed in R (http://cran.r-project.org).

Flow cytometric analysis of the B16.F10 TME. B16.F10 tumours were established subcutaneously in C57BL6/J mice, as previously described, and treated intratumorally with either PBS or co-formulations of cGAMP (10 μg) and cdGMP-Dy547 (0.2 μg). At 48 h after treatment, the tumours and inguinal draining lymph node were harvested, mechanically dissociated with an OctoMACS separator, and digested in a solution of 125 μg ml^{-1} Deoxyribonuclease I (Worthington) and 500 μg ml^{-1} Collagenase III (Worthington) in RPMI 1640 media for 30 min at 37 °C. Tumours and lymph nodes were strained through a 40 μm cell strainer and treated with ACK Lysing Buffer (Gibco). Cells were diluted to a concentration of 2×10^7 cells ml^{-1} in PBS containing 2% bovine serum albumin for staining with fluorescent antibodies. 100 μl of cell suspension for each flow test was transferred into a 96-well plate and treated with FcX (BioLegend) according to the manufacturer's specifications. Samples were stained with several panels of the antibodies BV650-αCD45 (30-F11), PE/Cy5-αCD11b (M1/70), PE-αCD11c (N418), PE/Cy7-αNK1.1 (PK136), APC/Cy7-αF4/80 (BM8), APC/Cy7-αMHC-II (10.3.6), PE-αCD206 (C068C2), APC-αCD86 (GL-1), APC-αCD3 (17A2), APC/Cy7αCD4 (RM4-5) and PE/Cy5-αCD8α (53.6.7) (BioLegend). BV, brilliant violet; PE, phycoerythrin; Cy, cyanine; APC, allophycocyanin. Cells were washed twice, suspended in PBS containing 2% FBS and 200 nM 4′,6-diamidino-2-phenylindole before analysis on a BD LSRFortessa or BD LSR II flow cytometer (Supplementary Fig. 14).

For intracellular cytokine analysis, 10^6 cells were seeded in a 6-well plate in Dulbecco's modified Eagle's medium containing 10% FBS and supplemented with a PMA/ionomycin/Brefeldin A cocktail (BioLegend) according to the manufacturer's specification. After 4 h, the cells were washed, stained with antibodies against CD3, CD4 and CD8α, fixed with fixation buffer (BioLegend) and subsequently stained intracellularly with antibodies against TNF-α (MP6-XT22), IFN-γ (XMG1.2), IL-4 (11B11) and IL-10 (JES5-16E3) (BioLegend) in Intracellular Staining Permeabilization Wash Buffer (BioLegend). All flow cytometry data were analysed using FlowJo software (version 10; Tree Star; https://www.flowjo.com/solutions/flowjo).

Treatment of B16.F10 subcutaneous tumours. 5×10^4 B16.F10 cells were injected subcutaneously into the flank of 6–8-week-old mice in 100 μl of serum-free RPMI 1640 media. The tumour size was measured every other day via calliper measurements, and the tumour volume calculated using the equation $V=\frac{1}{2}\times L\times W\times H$. On reaching sizes of ~100 mm^3, tumours were treated intratumorally with 100 μl of PBS containing 10 μg of 2′3′-cGAMP in various formulations. Mice were euthanized at a tumour burden endpoint of 1,500 mm^3. For single tumour models, on reaching a tumour volume of ~100 mm^3, tumours were injected intratumorally with 100 μl of the appropriate formulation in pH 7.4 PBS. Mice were injected 3× with treatments spaced 4 d apart. For contralateral studies, mice were inoculated on each flank subcutaneously. When the larger of the two tumours reached ~100 mm^3, it was injected with 100 μl of the appropriate formulation and designated as the primary tumour, with the untreated tumour designated as the contralateral tumour. Mice treated with checkpoint blockade were injected intraperitoneally with 100 μl of PBS containing 100 μg of both anti-PD-1 (RMP1-14; Bio X Cell) and anti-CTLA-4 (9D9; Bio X Cell). Treatments were spaced 4 d apart. For evaluation via systemic administration, mice were injected in the caudal vein with 100 μl of PBS containing the appropriate formulation 7 d following a tumour inoculum of 5×10^5 B16.F10 cells (average volume = 30 mm^3). Treatments were spaced 4 d apart.

Analysis of blood chemistry and hepatocellular toxicity. On reaching the tumour size endpoint, blood was harvested via submandibular bleeding, allowed to clot, and used to prepare serum by centrifugation at 4,000*g*. The serum was tested by the Vanderbilt Translational Pathology Shared Resource for levels of alanine aminotransferase, bilirubin and creatinine. Livers were harvested, fixed in a 10% formalin in PBS solution, paraffin embedded and sectioned into 5 μm sections for haematoxylin and eosin staining. Interpretation was completed by a board-certified veterinary pathologist under masked conditions.

Ex vivo stimulation of resected human metastatic melanoma. All experiments using human samples were performed in compliance with United States Federal Policy for the Protection of Human Subjects and guidelines set forth by the Vanderbilt University Human Research Protections Program. Experiments were approved by the Vanderbilt University Institutional Review Board, and all patients were consented for research use of biospecimens (Vanderbilt University Medical Center IRB number 030220). Within one hour of surgical resection at Vanderbilt University Medical Center, human melanoma tumours were submerged in Dulbecco's modified Eagle's medium/F12 media (Gibco) supplemented with 10% FBS, and divided into nine sections using a scalpel. Individual sections were then placed in a 12-well plate containing 1 ml of media and injected with STING-NP, free cGAMP or PBS using a syringe, reaching a final concentration of 100 ng ml^{-1} of cGAMP within each well. 24 h after treatment, RNA isolation, cDNA synthesis and qPCR analysis were then performed as described previously. The TaqMan gene expression kits were: Hs00174128_m1 for human *Tnf*; Hs01077958_s1 for human *Ifnb1*; Hs00171042_m1 for human *Cxcl10*; and Hs00609296_g1 for human *Hmbs*.

Statistical analysis. All statistical analyses were performed using GraphPad Prism software, version 7.0 (https/graphpad.com/scientific-software/prism).

Reporting Summary. Further information on research design is available in the Nature Research Reporting Summary linked to this article.

Data availability

The data that support the findings of this study are available from the corresponding author upon reasonable request.

References

54. Ghosh, S., Basu, S. & Thayumanavan, S. Simultaneous and reversible functionalization of copolymers for biological applications. *Macromolecules* **2006**, 5595–5597 (2006).
55. Matini, T. et al. Synthesis and characterization of variable conformation pH responsive block co-polymers for nucleic acid delivery and targeted cell entry. *Polym. Chem.* **5**, 1626–1636 (2014).
56. Gaffney, B. L., Veliath, E., Zhao, J. & Jones, R. A. One-flask synthesis of c-di-GMP and the [Rp,Rp] and [Rp,Sp] thiophosphate analogues. *Org. Lett.* **12**, 3269–3271 (2010).

nature research

Corresponding author(s): John T. Wilson

Reporting Summary

Nature Research wishes to improve the reproducibility of the work that we publish. This form provides structure for consistency and transparency in reporting. For further information on Nature Research policies, see Authors & Referees and the Editorial Policy Checklist.

Statistical parameters

When statistical analyses are reported, confirm that the following items are present in the relevant location (e.g. figure legend, table legend, main text, or Methods section).

n/a	Confirmed	
☐	☒	The exact sample size (*n*) for each experimental group/condition, given as a discrete number and unit of measurement
☐	☒	An indication of whether measurements were taken from distinct samples or whether the same sample was measured repeatedly
☐	☒	The statistical test(s) used AND whether they are one- or two-sided *Only common tests should be described solely by name; describe more complex techniques in the Methods section.*
☒	☐	A description of all covariates tested
☒	☐	A description of any assumptions or corrections, such as tests of normality and adjustment for multiple comparisons
☐	☒	A full description of the statistics including central tendency (e.g. means) or other basic estimates (e.g. regression coefficient) AND variation (e.g. standard deviation) or associated estimates of uncertainty (e.g. confidence intervals)
☐	☒	For null hypothesis testing, the test statistic (e.g. *F*, *t*, *r*) with confidence intervals, effect sizes, degrees of freedom and *P* value noted *Give P values as exact values whenever suitable.*
☒	☐	For Bayesian analysis, information on the choice of priors and Markov chain Monte Carlo settings
☒	☐	For hierarchical and complex designs, identification of the appropriate level for tests and full reporting of outcomes
☒	☐	Estimates of effect sizes (e.g. Cohen's *d*, Pearson's *r*), indicating how they were calculated
☐	☒	Clearly defined error bars *State explicitly what error bars represent (e.g. SD, SE, CI)*

Our web collection on statistics for biologists may be useful.

Software and code

Policy information about availability of computer code

Data collection	Flow cytometry data was collected using FACSDiva software (v6.1.3). IVIS; Living Image software (v4.5). TEM; Gatan DigitalMicrograph (v2.12.1579.0), TIA (v4.7), Tecnai Osiris (v4.6.4). PCR; CFX Manager (v.3.1). NMR (Topspin, v.3.5). GPC; Astra (v5.3.4). DLS/zeta (Zetasizer v.7.12). Plate based absorbance, luminescence, and fluorescence assays; Gen5 (v2.06).
Data analysis	Statistical analyses were performed using GraphPad Prism software (v7). nanoString data was analyzed using nCounter software (v3.0) and R software package (v3.2). Flow cytometry data was analyzed using FlowJo software (v10). IVIS data was analyzed using Living Image software (v4.5).

For manuscripts utilizing custom algorithms or software that are central to the research but not yet described in published literature, software must be made available to editors/reviewers upon request. We strongly encourage code deposition in a community repository (e.g. GitHub). See the Nature Research guidelines for submitting code & software for further information.

Data

Policy information about availability of data

All manuscripts must include a data availability statement. This statement should provide the following information, where applicable:

- Accession codes, unique identifiers, or web links for publicly available datasets
- A list of figures that have associated raw data
- A description of any restrictions on data availability

The data that support the findings of this study are available from the corresponding author upon reasonable request.

Field-specific reporting

Please select the best fit for your research. If you are not sure, read the appropriate sections before making your selection.

☒ Life sciences ☐ Behavioural & social sciences ☐ Ecological, evolutionary & environmental sciences

For a reference copy of the document with all sections, see nature.com/authors/policies/ReportingSummary-flat.pdf

Life sciences study design

All studies must disclose on these points even when the disclosure is negative.

Sample size	Sample sizes were estimated to achieve 90% power for detection of significant differences in tumor volume between groups based on means and standard deviations estimated in preliminary studies and were consistent with sample sizes used in similar reports in the literature.
Data exclusions	No samples were excluded.
Replication	Each experiment was replicated once unless otherwise indicated in figure caption, and conclusions drawn from the data in each experiment were consistent.
Randomization	Mice were randomly sorted into treatment and control groups. In tumor studies, tumor volume was measured prior to initiation of treatment to ensure the same mean volume across cohorts.
Blinding	Tumor volume measurements and raw data generation from tumor models were performed by independent researchers who were blinded as to treatment group assignment.

Reporting for specific materials, systems and methods

Materials & experimental systems

n/a	Involved in the study
☒	☐ Unique biological materials
☐	☒ Antibodies
☐	☒ Eukaryotic cell lines
☒	☐ Palaeontology
☐	☒ Animals and other organisms
☐	☒ Human research participants

Methods

n/a	Involved in the study
☒	☐ ChIP-seq
☐	☒ Flow cytometry
☒	☐ MRI-based neuroimaging

Antibodies

Antibodies used	All antibodies used in flow cytometry were obtained from Biolegend against: CD45(30-F11, 103108). CD11b (M1/70, 101209), Ly6C(HK1.4, 128015), F4/80 (BM8, 123117), CD206 (C068C2, 141705), CD86 (GL-1, 105014), CD11c (N418, 117307), I-A/I-E (M5/114.15.2, 107627), CD8a (53-6.7, 100710), CD4 (GK1.5, 100414), CD3 (17A2, 100236), NK1.1 (PK136, 108707), IFN-g (XMG1.2, 505807), TNF-a (MP6-XT22, 506315), Ly6G (1A8, 127625), IL-4 (11B11), IL-10 (JES5-16E3). Flow cytometric antibodies were used at a 1:100 dilution. Therapeutic antibodies were obtained from Bio X Cell against: CTLA-4 (9d9, BE0164), PD-1 (RMP1-14, BE0146). Lot numbers were not recorded.
Validation	Flow cytometric antibodies were validated by Biolegend using bone marrow cells or splenocytes from C57BL/6 mice. Related data is shown on the manufacturer website. Therapeutic antibodies were validated by SDS-PAGE by BioxCell, with relevant data

presented on the manufacturer website. Additional validation of both therapeutic and flow cytometric antibodies was not performed by the authors.

Eukaryotic cell lines

Policy information about cell lines

Cell line source(s)	B16.F10 murine melanoma cells were provided by Dr. Barbara Fingleton (Vanderbilt University) and originally obtained from American Type Culture Collection (ATCC; Manassas, VA, USA). DC2.4 cells were provided by Prof. Kenneth Rock (University of Massachusetts Medical Center). B16-Blue ISG, THP1-Blue ISG, and RAW-Blue ISG reporter cells were purchased from Invivogen (San Diego, CA, USA).
Authentication	The cell lines used were not authenticated by the authors
Mycoplasma contamination	All cell lines used in this paper tested negative for mycoplasma.
Commonly misidentified lines (See ICLAC register)	No commonly misidentified cell lines were used.

Animals and other organisms

Policy information about studies involving animals; ARRIVE guidelines recommended for reporting animal research

Laboratory animals	Experiments and handling of mice were conducted under federal, state, and local guidelines and with approval from the Vanderbilt University IACUC. Six to eight week old female C57Bl/6 mice were purchased from the Jackson Laboratory.
Wild animals	The study did not involve the use of wild animals.
Field-collected samples	The study did not involve samples collected from the field.

Human research participants

Policy information about studies involving human research participants

Population characteristics	Surgically resected melanoma specimens were obtained from two patients under Vanderbilt University Medical Center IRB 030220 - "Melanoma, Pigmented Lesion and Cutaneous Malignancy Tissue and Biospecimen Repository." Subjects with lesions in any of the nine steps in melanoma progression are eligible to participate. All subjects give informed consent. All tissue specimens are de-identified.
Recruitment	Eligible patients were be invited to participate by one of the investigators or a designee of one of the investigators. If they are willing to participate, the investigator or their designee reviewed the consent form and obtained informed consent. All patients with melanoma with planned surgery were consented to the melanoma tissue collection protocol. Patients were approached in clinic by study personnel without relation to age, race, gender, disease stage, or prior therapies. Patients with tissue collected tended to have more extensive disease involvement (thus having leftover tissue for research); otherwise no significant biases appeared to be present.

Flow Cytometry

Plots

Confirm that:

☒ The axis labels state the marker and fluorochrome used (e.g. CD4-FITC).

☒ The axis scales are clearly visible. Include numbers along axes only for bottom left plot of group (a 'group' is an analysis of identical markers).

☒ All plots are contour plots with outliers or pseudocolor plots.

☒ A numerical value for number of cells or percentage (with statistics) is provided.

Methodology

Sample preparation	Tumors and lymph node samples were harvested from sacrificed mice, placed in RPMI 1640 supplemented with DNAse I and Collagenase III (Worthington) at concentrations of 125 ug/mL and 500 ug/mL, respectively. Tissues were mechanically disrupted using an gentleMACS tissue dissociator (Mitenyi), followed by incubation at 37C for 1 hour. Samples were then passed through a 40 um cell strainer and exposed to ACK lysing buffer (Gibco) for 5 minutes before resuspension in PBS FACS buffer containing 2% BSA. Samples were stained with the appropriate antibodies for 30 minutes at 4C in the dark, washed, and resuspended in FACS buffer containing 200 nM DAPI for analysis. Uptake of Dy547 was analyzed using a 561 nm yellow green laser. For intracellular cytokine staining, single cell suspensions of tumors were plated in 6 well plates containing DMEM supplemented with 10% FBS and treated with brefeldin A and PMA/ionomycin (Biolegend) used according to manufacturer specifications. 4 hours later, cells were stained with antibodies against CD3, CD4, and CD8a, fixed with Biolegend Fixation Buffer, and subsequently stained intracellularly with antibodies against TNF-a and IFN-g in the presence of Biolegend Permeabilization

	Buffer. Following 30 minutes of staining, cells were washed 2x with Biolegend Permeabilization Buffer and resuspended in FACS buffer for flow cytometric analysis.
Instrument	LSRFortessa, BD LSR II
Software	Data collection: FACSDiva v6.1.3. BD. Data Analysis: FlowJo v10, Tree Star, Inc.
Cell population abundance	No sorting was performed
Gating strategy	Doublets and debris were excluded from sample analysis by FSC/SSC discrimination. Dead cells were subsequently excluded using DAPI before further analysis. Gates were drawn to demarcate cell populations with clearly distinct levels of fluorescence or size characteristics to discriminate between cell types. For characterization of percentages of cells producing intracellular cytokines or uptaking fluorescent Dy547, gates were drawn such that negative controls (PBS treated cells in both cases) yielded a negligible population of cells positive for the targeted markers. Representative gating strategies are shown in the Supplementary Information.

☒ Tick this box to confirm that a figure exemplifying the gating strategy is provided in the Supplementary Information.